

Effects of the mechanical wave propagating in the wind direction on currents and stresses across the air–water interface

Shinjiro Mizuno

*Former: Department of Civil Engineering, Hiroshima Institute of Technology, Japan;
present address: Hatsuka-ichi city, Miyajima-guchi-Higashi 1-2-1, Hiroshima, Japan,
E-mail: sinmizuno@yahoo.co.jp*

Abstract. Vertical/cross-wind profiles of current velocities were measured at a constant wind speed of about 8 m/s with a two-component Laser Doppler anemometer. By adding mechanical waves in the wind direction, the resulting current profiles were measured and compared with those for wind-only case at the same wind speed. Development of Langmuir circulation (LC) was compared to each other for 2 wind and wave experiments: Case 1 for pure wind-waves and Case 2 for wind plus mechanical waves. Only for Case 1 experiment, two-dimensional Langmuir Circulation (2D-LC) developed in a high lateral shear flow favorable to driving the Garrett's (1976) vortex force. For Case 2 experiment, addition of mechanical wave suppressed the Garrett's vortex force, leading to reduction of the wind-driven current and decay of the 2D-LC. Thus, response of the 2D-LC to the monochromatic wave differed considerably from results of Case 1 experiment, the laboratory experiment for CL I model of LC (Faller 1978), and recent numerical experiments for CL II model of LC (e.g., McWilliams *et al.* 1997).

Key Words: Langmuir circulations, Garrett's vortex force, wave-induced return flow.

1. Introduction

Wind and wave experiments were attempted for two cases at a wind speed of about 8 m/s. For the pure wind-wave experiment, downwind jets associated with a pair of two-dimensional Langmuir circulation (2D-LC) developed along the sidewalls of the tank (e.g., Mizuno and Cheng 1992). For the second case when mechanical waves propagated in the wind direction, the jets decayed with increasing wave slope ak and disappeared almost entirely for $ak=0.1$, where a and k denote the wave amplitude and wavenumber, respectively. Apparently, the latter experimental result seems to contradict prediction of CL II theory of Langmuir circulation (LC) (Craik 1977) and recent several numerical experiments of LC (e.g., McWilliams *et al.* 1997). For a better understanding of the wind-wave-current

coupling, the primary purpose of this paper is to reveal the development of 2D-LC for the pure wind-waves and its decay for the wind plus mechanical wave case in terms of two Stokes wave drift effects described below.

In the beginning we briefly review how the Lagrangian Stokes drift associated with waves affects the dynamics of wave-current interaction in the upper ocean mixed layer. Since theoretical study of Craik and Leibovich (1976), Craik-Leibovich (CL) vortex force has been widely known as the most effective wave effect that drives development of LC. In addition, there is another Stokes wave effect that is called Stokes-Coriolis force, which is the up-wave return drift induced by Stokes drift in the upper ocean (Hasselmann 1970). Polton *et al.* (2005) successfully applied the effect of Stokes-Coriolis force to the current profiles observed in the wind-driven upper ocean mixed layer. Accordingly, in recent studies of LC in the upper ocean these two additional Stokes drift terms, i.e., CL vortex force and Stokes-Coriolis force, are included in the momentum equations (e.g., McWilliams *et al.* 1997). The LC due to wave-current interaction is usually driven by either of CL I or II vortex force (Leibovich 1983):

$$(f_y^{CL}, f_z^{CL}) = \left(U_s \frac{\partial U}{\partial y}, U_s \frac{\partial U}{\partial z} \right) \quad (1.1)$$

where f^{CL} represents the vortex force, y and z the lateral and vertical coordinate components, and U and U_s are Eulerian mean flow and Stokes drift, respectively. CL I model is driven by the interaction of vertical shear and regular crossed-waves (Craik and Leibovich 1976), CL2 model driven by that of lateral shear and random or monochromatic progressive waves (Craik 1977). Faller (1978) and Faller and Cartwright (1983) have shown that wind plus mechanically generated crossed-wave experiments generally support CL I model. Their experiments have also made a favorable contribution to the validity of CL II theory. According to a review of Thorpe (2004), CL II model is likely to be widely accepted in many recent studies of LC in oceans and lakes.

This study is an extension of the Cheung and Street's (1988) laboratory experiments to two-dimensional cross-sectional measurements normal to the wind. Experiments consist of the following 3 runs: one run of pure wind-waves and 2 runs of wind plus monochromatic, mechanical wave (with different wave slopes) propagating in the wind direction. The former and latter correspond to Case I and II experiments of Cheung and Street (1988), thus being referred to hereafter as C1-EXP and C2-EXP, respectively. For each run, two-dimensional vertical structures of the primary and secondary flow were measured below the wave troughs at a wind speed of about 8 m/s using a two-component Laser Doppler anemometer (LDA). Because of page limit, we focus only on mean current velocities and turbulent shear stresses. Contrary to the above-mentioned recent experiments

favorable to CL I and II models, in this paper we report that the downwind jets associated with 2D-LC developed for C1-EXP but decayed for C2-EXP.

For C1-EXP, Mizuno and Cheng (1992) have found a pair of steady 2D-LC in a water tank. Even if qualitative, the 2D-LC seems to be controlled by CL II vortex force. Thereafter, the presence of 2D-LC is confirmed in several tanks (Mizuno *et al.* 1998; Matsunaga and Uzaki 2004; Dethleff and Kempema 2007). An idealized flow pattern of 2D-LC consists of faster, narrower downwelling jet region and slower, broader upwelling region (Pollard 1977). In addition, the parcels moving toward a downwelling region by LC in the near-surface layer are accelerated by the wind stress in the wind direction, thus attaining to the maximum downwind flow in the downwelling region. This downwind velocity jet is another characteristic feature of LC. Garrett's (1976) theory predicts formation of downwind jet associated with 2D-LC by the action of lateral vortex force, F_y^G , which equals the product of wave momentum M_s and mean shear $\partial U/\partial y$:

$$F_y^G = M_s \frac{\partial U}{\partial y}. \quad (1.2)$$

In section 3 we shall estimate the order of magnitude of downwind jets using (1.2).

For C2-EXP, Mitsuyasu and Honda (1982) have reported that mechanical waves grow exponentially with fetch by the action of wind within an initial fetch from 2 to about 10 m, and thereafter stop or decay their growth by the occurrence of wave breaking. But for the same C2-EXP, since Mitsuyasu's (1966) pioneering study, several peculiar wave effects are often reported: for example, addition of mechanical waves suppressed the wind-wave energy (Mitsuyasu 1966; Phillips and Banner 1974), made the water surface super-smooth (Hsu *et al.* 1982), reduced the air-side stress for wave steepness ak less than 0.2 (Makin *et al.* 2007), and damped CO₂ gas transfer across the air-water interface in the wind speed less than 9 m/s (Tanno and Komori 2004). Cheung and Street (1988) have also reported reduction of both downwind mean current and boundary layer thickness on the water-side by the mechanical wave.

In this laboratory experiment we found the Stokes wave effect dynamically similar to the Stokes-Coriolis force acting in the rotating flow. This effect is referred to as wave-induced return flow. As shown in section 3, the knowledge of this return flow as well as the Garrett's vortex force is highly important for a better understanding of wave-current interaction in a closed tank. To explain why the wave-induced return flow generates in the tank, let us consider steady flow under wind waves or monochromatic waves propagating in the wind direction in a closed tank. For simplicity, the flow is assumed laterally uniform. Since integration of the total momentum from the bottom D to the wave surface, η , requires the net flow flux = 0, we obtain

$$\int_{-D}^{\eta} u dz = \int_{-D}^0 U dz + \int_0^{\eta} \tilde{u} dz = M_E + \overline{(\tilde{u}\eta)}_0 = M_E + M_S (\text{or } M_W) = 0, \quad (1.3)$$

where $u = U + \tilde{u}$, u is the sum of mean current U and wave-induced component \tilde{u} of the downwind current velocity, M_E is the net Eulerian volume transport per unit width, and two Stokes wave transports, $M_S = \overline{(\tilde{u}\eta)}_0$ and $M_W = \overline{(\tilde{u}\eta)}_0$, are those associated with mechanical waves and wind waves, respectively. From the final equation of (1.3), we obtain

$$[U] = \frac{1}{D} \int_{-D}^0 U dz = -\frac{M_W}{D} \text{ for C1-EXP; } [U] = \frac{1}{D} \int_{-D}^0 U dz = -\frac{M_S}{D} \text{ for C2-EXP,} \quad (1.4a, 1.4b)$$

where $[\cdot]$ denotes the depth-mean quantity.

For C1-EXP, a greater part of the momentum flux associated with wind waves ($\sim 94\%$ of the wind stress) is transferred into wind-driven current (Toba 1978) and because of wave breaking most of the wind-wave momentum M_W is finally dissipated into heat by turbulent diffusion. That is, the transport of the downwind flow well balances that of the return flow, i.e., $[U] \approx 0$. On the other hand, for C2-EXP the wave momentum flux, dM_S/dt , is transferred largely into the growth of wave energy by the action of wind (Mitsuyasu 1985). Hence, if balance equation (1.4b) holds, a significant up-wave return flow must be set up in the tank to balance the Stokes wave drift. Thus, the depth-mean return flow, $[U]$, which is equal to $-M_S/D$ ($= -\omega a^2 \coth(kD)/2D$), is induced by the Stokes drift, where ω is the radian wave frequency. It seems that the above-mentioned peculiar wave effects across the air-water interface are associated closely with generation of the wave-induced return flow found for the present C2-EXP.

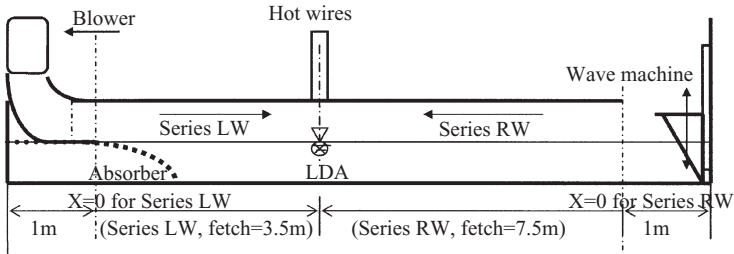
2. Experiments

Experiments were carried out in a wind-wave tank of Hiroshima Institute of Technology, Japan. Figure 1 gives a brief sketch of the wind and water tank used. Dimensions of the tank are as follows: the whole length 13 m, test section 11 m long, width $B = 30$ cm, water depth $D = 25$ cm, and height of the wind section $H = 30$ cm. A wind blower and a plunger type of wave maker were installed at the left and right end of the tank, as shown in Figure 1. Measurements were made at a fetch of 7.5 m from the right end of the test section at a constant wind speed of about $U_w = 8$ m/s.

Two series of experiments (series RW and LW) were conducted by changing the direction of wind to right and left, respectively. Wind direction was the same as

Table 1 Wind and wave conditions for series RW

Series RW	Wind Speed	Wind stress at $y=z=0$	Wave age	Wave amplitude	Wave slope	Stokes drift at surface
Parameter	U_w	τ_0	C/U_w	a	ak	$U_s(0)$
Unit	m/s	dynes/cm ²		cm		cm/s
C1-EXP	7.8	1.6	–	0	0	0
C2-EXP1	8.4	1.6	0.15	1.4	0.07	0.7
C2-EXP2	8.4	–	0.15	2.1	0.10	1.6

**Figure 1** Outline of the wind and water tank.

that of wave propagation for series RW (wind blowing from right) and opposite for series LW (wind blowing from left). In this paper we report results of 3 runs for series RW: C1-EXP and C2-EXP with 2 different slopes ak (C2-EXP1 and C2-EXP2). Table 1 indicates the experimental conditions for 3 runs, where a and ak indicate those of mechanical wave at the location of measurement.

Sinusoidal waves were generated by setting the stroke of the wave machine at 5 and 10 cm at a constant frequency, 1 Hz, thus $C=1.3$ m/s and $L=1.3$ m using dispersion relation of wave, where C and L is the phase speed and wave length. Direct measurements of wind and currents were made on both sides of the surface with an X-type hot-wires and a two-component Laser Doppler anemometer (LDA), respectively. The x -axis is positive in the downwind direction from the right end of the test section ($x=0$ in Figure 1). The origin of y -axis is at the centre, and that of the vertical z -coordinate is at still water surface and positive upwards. Instantaneous downwind and vertical currents (u , w) were decomposed into mean velocities (U , W) and turbulent fluctuations including wind-wave components (u' , w')

$$u(y, z, t) = U(y, z) + u'(y, z, t), \quad w(y, z, t) = W(y, z) + w'(y, z, t), \quad (2-1)$$

where $U(y, z)$ and $W(y, z)$ denote the time mean values averaged over the record length (204.8 sec). Wave-induced components (\tilde{u} , \tilde{w}) were used to calculate the wave amplitude a and surface Stokes drift $U_s(0)$ in Table 1, but excluded from

(2.1) because the wave-induced Reynolds stress was not used in this paper. The current velocities were measured with backward-scatter mode using a two-component LDA of TSI Incorporated, USA. A personal computer was used to automatically acquire the current data measured with the LDA mounted on a high precision of y - z traversing mechanism (pitch=0.1mm). They were obtained by traversing a y - z cross-section normal to the wind direction over the following range of measurement:

$$-0.47 \leq y/B \leq 0.47, \text{ and } -0.76 \leq z/D \leq -0.12.$$

Measurements were made at a total of 15 x 9 stations: laterally 15 points for each of 9 depths at an interval of 2 cm, about 1 hour after the onset of wind and waves to establish stationary flow state. The record time of (u , w) at each station was 204.8 sec (4096 sampling points), which included about 205 paddle waves (wave period=1 s), at a sampling frequency of 20 Hz. About 10 hours per one run were required to measure the total 135 stations.

3. Results and discussions

3.1 Vertical cross-sectional profiles of mean currents

Figure 2 shows iso-velocity contours of mean currents $U(y/B, z/D)$ and $W(y/B, z/D)$ in a vertical cross-section for all 3 runs. Among them we mostly compare the velocity contours of C1-EXP with those of C2-EXP2. Two panels (a) and (d) in Figure 2 show the primary and secondary circulations for C1-EXP. Note that they are very close to an idealized 2D-LC, or the famous Pollard's (1977) LC. The downwind jets (panel a) of high speed ($2 \sim 4$ cm/s) extended along the sidewalls downwards very deeply in the downwelling regions with downward speed of $1 \sim 2$ cm/s, and the downwind transport was sufficiently compensated for by that of undercurrent (dark grey area of U) that returned back through the central upwelling region (white and black area of W). Since the flow is laterally balanced, $\{U\} \approx 0$ holds, as indicated in Table 2, where $\{\cdot\}$ denotes the average value over the whole cross-section measured. Since the pattern of panel (a) is consistent with both CL II and Garrett's lateral vortex force associated with 2D-LC, it is certain that its formation is due to the wave-current interaction. In fact, it is evident that the primary circulation for C1-EXP differs greatly from that expected from two-layer model. The secondary circulation in panel (d) consists of downwelling flow along the sidewalls and a compensating upwelling flow in the centre region, confirming our previous result for wind-only case (Mizuno and Cheng 1992; Mizuno *et al.* 1998).

Next compare panel (a) and panel (c) for C2-EXP2 with $ak=0.1$ then it is evident that the mechanical wave caused a catastrophic collapse of the 2D-LC. That is, the region of downwind velocity jets disappeared entirely for C2-EXP2,

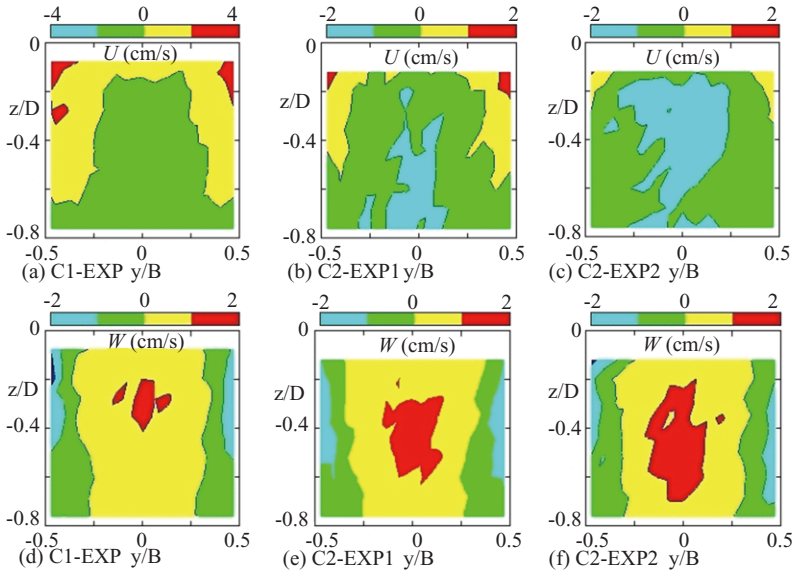


Figure 2 Vertical/cross-wind profiles of U (top panels) and W (bottom panels) current components. (a),(d), C1-EXP; (b), (c) and (e), (f), two C2-EXP. White and black area indicate the downwind and upward velocity region, while dark and light grey area the return current and downward velocity region, respectively. Note that only the scaling of U for panel (a) is twice as large as others. The square marks in the bottom panels indicate the curves of $W=0$.

except near the upper corners. Simultaneously a greater part of the whole water column was occupied by the region of reverse undercurrent, as shown in panel (c). The resulting downwind transport extremely decreased compared with that of the return flow. What caused this drastic change in volume transport? Since almost all of the water column was occupied by return flow by adding wave, we should consider that the wave-induced return flow totally dominated over CL II or Garrett’s vortex force. Note that, as indicated in columns 2 and 3 of Table 2, the lateral-mean Eulerian transport per unit width, $\langle M_E \rangle$, for C2-EXP is not satisfied by $\langle M_E \rangle \approx 0$ but approximately balanced by the lateral-mean Stokes mass transport per unit mass, $\langle M_S \rangle$, associated with the mechanical wave.

Three bottom panels in Figure 2 show the secondary circulation. The wave effect on the secondary flow was much less than that on the primary flow, though upwelling current in the centre region increased slightly with increasing ak (see black mark of W). Steady secondary flow was observed for all runs measured, but this does not mean that all secondary flow is 2D-LC. Panel (d) can be regarded as 2D-LC because the wind-driven lateral flow near the surface produced significant downwind jets (see panel (a)). However, that of panels (e) and (f) is sidewall effect because it is not wind-driven but primarily due to the wave-induced return flow

(compare each panel with the corresponding top one).

3.2 Variation of the primary flow with wave slope ak

Figure 3 shows how the primary flow changes with wave slope ak . Figure 3a compares vertical profiles of twice the energy of horizontal mean velocity, $U^2(z)$, at $y/B=0$ and those at $|y/B|=0.467$. At $|y/B|=0.467$, the vertical profile of $U^2(z)$ for C1-EXP decreased rapidly from the largest value near the surface toward the bottom, whereas at $y/B=0$ it increased from the surface to the bottom. This indicates that the downwind jet flow of high speed along the sidewalls returns back as the undercurrent at the center. For C2-EXP it should be noted that the kinetic energy of the primary flow became extremely weaker with disappearance of the downwind jets than that for C1-EXP.

Figure 3b shows vertical profiles of lateral mean current, $\langle U(z) \rangle$, for series RW. For C1-EXP, note that the high shear flow of $\langle U(z) \rangle$ was produced by the downwind jets, and that the downwind transport in the upper half layer well balances that of the return flow in the lower half layer, i.e., $\{U\} \approx 0$. For C2-EXP, the Eulerian balance of $\{U\} \approx 0$ tends to be broken with increasing ak . That is, Figure 3b shows the transition of volume transport balance from $\{U\} \approx 0$ to $\{U\} \approx -M_s/D < 0$ with increasing wave slope ak .

Next let us evaluate the wind and wave effects in the top 3 panels of Figure 2. We estimated $M_{dw}(y)$, $M_{re}(y)$, and Stokes-drift transport $M_s(y)$ at 15 lateral stations to assess the transport balance equations (1.4a) and (1.4b). They are plotted in Figure 4, where $M_{dw}(y)$ and $M_{re}(y)$ correspond to (+) and (-) portions (i.e., downwind and return flow) of the total Eulerian transport $\langle M_E \rangle$, respectively, and $M_s(y) = (\bar{u}\bar{\eta})_0$ was obtained by extrapolating using linear wave theory to the surface the \tilde{u} component of current data at $z = -3\text{cm}$. In panels (b) and (c) of

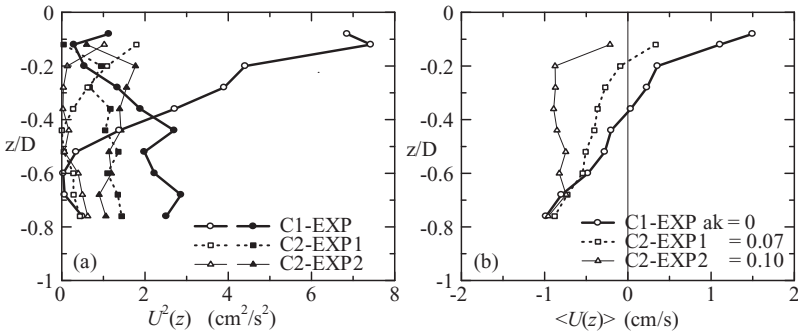


Figure 3 Vertical profiles of the primary flow for series RW. (a), vertical profiles of $U^2(z)$ at $y/B=0$ (solid symbols) and those at $|y/B|=0.467$ (open symbols), where the current data at $y/B=0$ are the average value of 3 data at the centre and its adjacent points; (b), vertical profiles of the mean current flow $\langle U(z) \rangle$ averaged over 15 lateral stations.

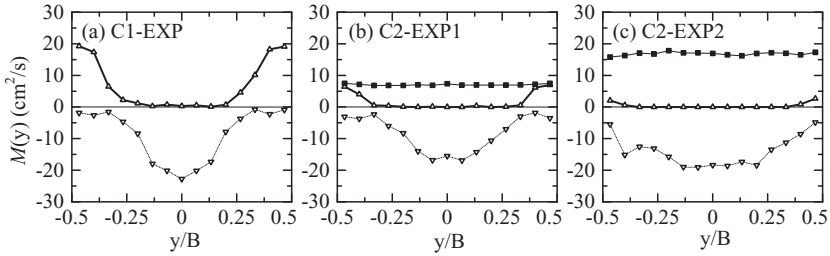


Figure 4 Lateral profiles of transport $M(y/B)$ as a function of y/B for U profiles in Figure 2. Symbols, (Δ) and (∇), are the transports, $M_{dw}(y)$ (bold solid lines) and $M_{re}(y)$ (dotted lines), respectively. The symbol (\blacksquare) in panels (b) and (c) denotes the Stokes wave transport, $M_s(y)$.

Table 2 Lateral mean values of Stokes and Eulerian transports in figure 4, and overall mean Stokes and Eulerian drift current.

Series	Stokes Transport	Eulerian Transport	Downwind Transport	Return Transport	Stokes drift Transport/D	Eulerian Drift	Drift ratio
RW	$\langle M_s \rangle$	$\langle M_{re} \rangle$	$\langle M_{dw} \rangle$	$\langle M_{re} \rangle$	$\langle M_s \rangle / D$	$\{U\}$	$\langle M_s \rangle / D / \{U\} $
Unit	cm ² /s	cm ² /s	cm ² /s	cm ² /s	cm/s	cm/s	%
C1-EXP	–	–0.6	8.2	–8.8	–	–0.03	–
C2-EXP1	7.1	–6.6	1.7	–8.3	0.28	–0.38	74
C2-EXP2	16.8	–13.3	0.4	–13.8	0.67	–0.77	87

Figure 4, $M_s(y)$ may have estimated higher than reality because the correlation coefficient between \tilde{u} and η was taken equal to 1. Table 2 summarizes the lateral mean values of transports in Figure 4 and their cross-sectional mean values of the Stokes-drift and Eulerian flow transports.

Figure 4 clearly shows that for C1-EXP, M_{dw} close to the sidewalls well balances M_{re} over the center region, whereas for C2-EXP, M_{re} is balanced not by M_{dw} but by M_s , and that M_{dw} becomes much larger only for C1-EXP. Fifteen data at $z = -2\text{cm}$ were added only for C1-EXP, and they are included in all transports in Figure 4 and $\{U\}$ in Table 2. Table 2 indicates that the volume transport balance is $\langle M_{dw} \rangle \approx \langle |M_{re}| \rangle$ for C1-EXP, but that $\langle M_s \rangle \approx \langle |M_{re}| \rangle$ for two C2-EXP. For the latter case, $\{U\} = -\langle M_s \rangle / D$ is approximately satisfied as indicated in the final column; the ratio $\langle M_s \rangle / (D|\{U\}|)$ is 74% and 87% for C2-EXP1 and C2-EXP2, respectively, where $\{U\}$ denotes the mean value of U at all stations measured. Although this ratio is a little smaller than 1, if the downwind current data in the wave boundary layer are included in $\{U\}$, it is expected that the value of $\{U\}$ approaches to $-\langle M_s \rangle / D$.

Now we estimate that the positive $M_{dw}(y)$ in Figure 4a (bold solid lines with symbol Δ), i.e., presence of the downwind jets for C1-EXP, which is due to the Garrett’s (1976) vortex force. After multiplying (1.2) by ρ_w/D , its integration from

z_0 to mean water surface $z=0$, yields

$$\int_{z_0/D}^0 \rho_w F_y^G dz = \frac{\rho_w M_w}{D} \frac{\partial M_{dw}}{\partial y}, \text{ where } M_{dw}(y) = \int_{z_0}^0 U(y, z) dz, \quad (3.1)$$

where z_0 denotes the depth at $U(y, z_0)=0$, U is assumed to be a function of y and z coordinates, and ρ_w is the density of water. In particular, note that M_s in (1.2) is replaced by M_w , the Stoke wave transport associated with wind waves, in (3.1).

For C1-EXP, let us evaluate the order of magnitude on the right-hand side of (3.1). Following Smith (2006), we estimated $\rho_w M_w$ as 2.9 g/cm \cdot s from the power spectrum of wind waves with a spectral peak at 3 Hz and about 2.8 cm/s as $\partial M_{dw}/\partial y$ from Figure 4a. Thus, the right-hand side of (3.1) gives the stress of 0.32 dynes/cm 2 , which amounts to 20 % of the wind stress (1.6 dynes/cm 2) extrapolated to the surface (see Table 1). Since there is a pair of LC in the tank, the total Garrett's vortex force is twice F_y^G and equal to 40 % of the wind stress. Next, Figure 4 also shows that both M_{dw} and $\partial M_{dw}/\partial y$ are much less for C2-EXP than C1-EXP because CL II and Garrett's vortex force, (3,1), were suppressed by wave-induced return flow. It follows that the present experimental results do not always contradict Garrett's mechanisms, if it is recognized that the wave-induced return flow dynamically dominated over the Garrett's vortex force for C2-EXP.

In summary, for C1-EXP the interaction between M_w associated with the wind wave and the high lateral shear, i.e., the Garrett's vortex force, enhanced the downwind jets close to the sidewalls, whereas for C2-EXP the wave-induced return flow, which was set up to balance the Stokes mass transport associated with the mechanical wave, suppressed the Garrett's vortex force, and then led to lower lateral shear and a rapid decay of the preexisting downwind jets with an increase of ak .

3.3 Variation of the secondary flow with ak

As shown in Figure 5a, the response of $W(z)$ profile to the mechanical wave was much weaker than that of $U(z)$. When the wave was added, at $|y/B|=0.467$ W slightly decreased in the near-surface layer but increased in the bottom half layer, whereas at $y/B=0$ W remained unchanged in the upper half layer but increased in the bottom half layer. This suggests that the centre of the secondary circulation shifted by about 5cm downwards with disappearance of the downwind jets probably because of reduction of the surface stress (see Figure 6). Although the center of secondary flow shifted downwards, its magnitude remained unchanged. Thus, it does not seem that the mechanical wave greatly changed the magnitude of the secondary flow.

Figure 5b shows lateral profiles of depth-mean current, $[W]$. Downwelling jets

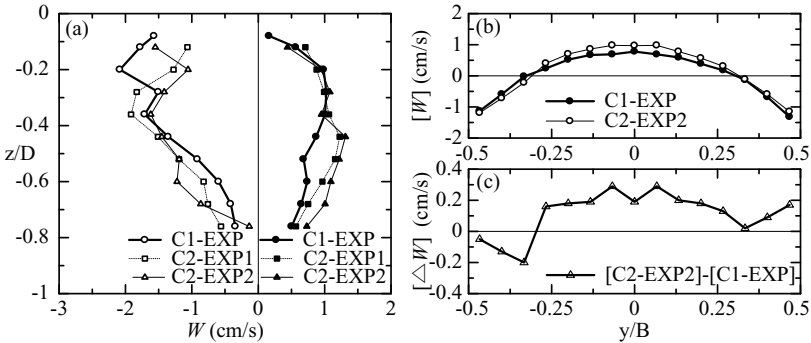


Figure 5 Secondary flow for series RW. (a), Vertical profiles of W at $y/B=0$ (solid symbols) and at $|y/B|=0.467$ (open symbols); (b), Lateral profiles of depth-mean current $[W]$ for C1-EXP and C2-EXP2; (c), Lateral profile of extra upwelling, $[\Delta W]$, which equals the difference of the two current data in panel (b): $[C2-EXP2]$ minus $[C1-EXP]$.

along the sidewalls remained almost unchanged independently of whether the wave is present or not. This result differs greatly from the Polton and Belcher's (2007) numerical result because their Figure 7 shows that the downwelling jets penetrated downwards very deeply by adding the wave. For C1-EXP the lateral mean value of $[W]$ was nearly zero, the maximum downwelling of about 1.2 cm/s slightly larger than the maximum upwelling of 0.8 cm/s at the centre. Thus the secondary flow for C1-EXP can be regarded as 2D-LC as mentioned earlier. In contrast, for C2-EXP2 an extra upwelling current was observed close to the center. Figure 5c shows the difference of $[W]$ between the two runs, about 0.2 cm/s over the centre region, which is considerably large as compared to the maximum upwelling of 0.8 cm/s for C1-EXP. We interpret that this extra upwelling is due to the vertical component associated with the wave-induced return flow rather than that associated with the secondary flow. Its generation is one reason why the water-side boundary layer thickness becomes much thinner for C2-EXP than C1-EXP (Cheung and Street 1988).

3.4 Variation of the air-side and water-side stresses with ak

Figure 6 shows both vertical/cross-wind profiles of the stresses measured above and below the surface and vertical profiles of their lateral mean stresses. The air-side stress was measured for C1-EXP and C2-EXP1 alone. The wave reduced the water-side stress greatly and widely enough to extend its effect over most of the whole depth, compared to the stress on the near-surface air-side. Thus the wave-induced return flow much more affects the water-side than near-surface air-side stress, suggesting that reduction of the air-side stress by the wave is partly due to the feedback effect from water-side. For C1-EXP, a greater part of wind

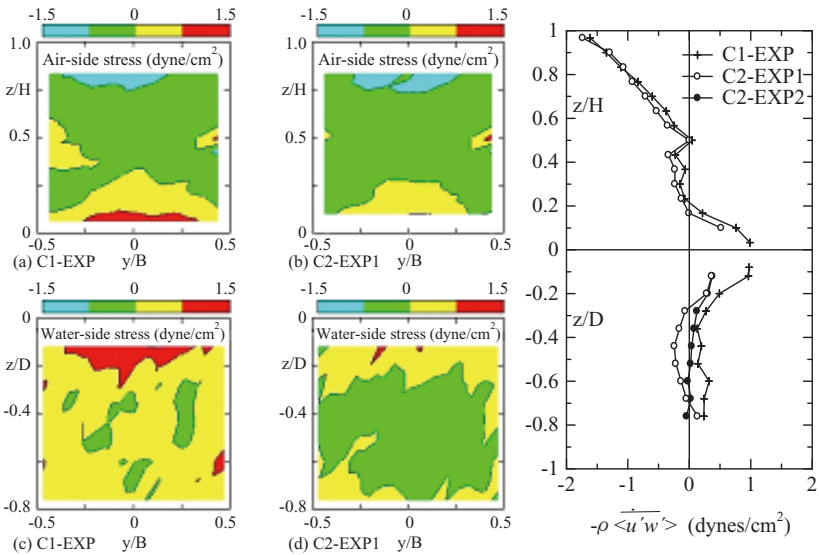


Figure 6 Vertical/cross-wind profiles of stresses. Air-side panels (a) and (b); water-side panels (c) and (d). Right panel, lateral-mean vertical profiles of the stresses in unit of dynes/cm².

momentum is injected into water closer to the centre than sidewalls, but a greater part of water was carried downwards along the sidewalls (see panel (a) of Figure 2). In contrast, for C2-EXP when the 2D-LC decayed, the water-side stress and return flow both became nearly laterally uniform with increasing ak .

4. Comparison with other studies

After a brief comment on the Cheung and Street's experiments (1988), we discuss how different the present experimental results favorable to the Garrett model are from the representative numerical simulation results of CL II model and the Faller's (1978) experiment of CL I model.

Cheung and Street (1988) emphasized that for their C2-EXP experiment, both wind-driven mean flow and boundary layer thickness on the water-side decrease by adding the mechanical wave in the wind direction, compared with those for their C1-EXP. They attributed its cause to an increase of the Karman constant, κ , in the logarithmic velocity profile. In contrast, Figure 6 clearly shows that its cause is reduction of the water-side Reynolds shear stress.

Next the present results in section 3 are compared in some detail with the numerical experiments of McWilliams *et al.* (1997) because their numerical results on three-dimensional Langmuir turbulence differed greatly from the present laboratory ones, although the driving force of the flow was common in

both studies, i. e., CL II vortex force and wave-induced return flow. They conducted 2 cases of wind and wave experiments very similar to the present experiments under the influence of the Earth’s rotation; C1-EXP, the turbulent flow due to surface shear stress without waves (S/∞); C2-EXP, the wind-driven flow under monochromatic waves propagating in the wind direction ($S/0.3$). As shown in Figure 2 of McWilliams *et al.* (1997), for C1-EXP a high shear flow was produced by the surface stress without generation of LC because of no waves, whereas for C2-EXP, the upper mixed layer became shear-free because of vigorous mixing of three-dimensional Langmuir turbulence by adding monochromatic wave. The wave had quite an adverse effect on the flow for the monochromatic wave between the numerical and laboratory studies, as shown below.

Two large differences were found in the development of LC for C2-EXP. First, in the laboratory study the downwind jets developed for C1-EXP with high lateral shear flow favorable to driving the Garrett’s vortex force but decayed rapidly for C2-EXP with reduction of the lateral shear, whereas in the numerical study the Langmuir turbulence driven by CL vortex force developed for C2-EXP in shear-free return flow, although the two C2-EXP had a common feature, $\{U\} \approx -M_s/D$, where D denotes the depth of mixed layer for the numerical study. Second, the largest difference between the two studies is in the water-side shear stress. McWilliams *et al.* (1977) assumed the surface stress to be equal to the wind stress, independently of whether the wave is present or not (see their Figure 3a). This makes a sharp contrast to our stress results in Figure 6 because for our C2-EXP, generation of the wave-induced return flow greatly reduced the water-side stress. This difference suggests that the growth rate of wave energy is an important factor that greatly affects the surface stress. The wave grew exponentially with fetch in the tank by the action of wind (Mitsuyasu and Honda 1982). In contrast, the wave amplitude is kept constant in the numerical study, indicating that there was no direct wave momentum flux into water.

The mechanically generated, crossed-wave experiments of Faller (1978) and Faller and Cartwright (1983) supported CL I model. Why does the wave-current interaction differ between CL I and CL II model? The following is a plausible answer to this question. Note that the downwelling regions of CL I model form along nodal lines of regular crossed-waves (see Craik and Leibovich 1976), where the wave amplitude vanishes. Because of no waves, no peculiar wave effects found for C2-EXP will occur along these nodal lines. Consequently, the wind momentum is more effectively injected into water at the nodes than antinodes of crossed-wave. Since the centre line of the tank is one of the nodal lines, it follows from Figure 6 that a greater part of the wind momentum is injected along the centre line and increases the downwind current there. Thus, it turns out that the wind

momentum is input directly into the downwind current jet developing in the central downwelling region. Further study is, of course, desirable for a better understanding of the air-water interaction for crossed-wave experiment.

Acknowledgements

The author thanks to Emeritus Professor of Kyushu University H. Mitsuyasu for his helpful advice for improving the manuscript and also to both graduate fellow M. Tokuchi and undergraduate student H. Kimura for their assistance to the experiments. This work was supported financially by the First High Technology and Second Research Projects of Hiroshima Institute of Technology and by Grant-in-Aid for Scientific Research (C) of the Ministry of Education, Culture, Sports, Science and Technology in Japan (RN.5540424).

References

- Craik, A.D.D.(1977) The generation of Langmuir circulations by an instability mechanism. *J. Fluid Mech.* 81, 209-223.
- Craik, A.D.D.and S. Leibovich (1976) A rational model for Langmuir circulations, *J. Fluid Mech.* 73, 401-426.
- Dethleff, D. and E. W. Kempema (2007) Langmuir circulation driving sediment entrainment into newly formed ice, *J. Geophys. Res.* 112, C02004, 1-15.
- Faller, A. J. (1978) Experiments with controlled Langmuir circulations. *Science*, 201, 618-620.
- Faller, A. J., R. and W. Cartwright (1983) Laboratory studies of Langmuir circulations. *J. Phys. Oceanogr.*, 13, 329-340.
- Garrett, C., (1976) Generation of Langmuir circulations by surface waves—a feedback mechanism, *J. Mar. Res.*, 34, 117-130.
- Hasselmann, K., (1970) Wave-driven inertial oscillation, *Geophys. Fluid Dyn.*, 1, 463-502.
- Hsu, C. T., H. W. Wu, E. Y. Hsu, and R. L. Street (1982) Momentum and energy transfer in wind generation of waves, *J. Phys. Oceanogr.*, 12, 929-951.
- Leibovich, S. (1983). The form and dynamics of Langmuir circulations, *Annu. Rev. Fluid Mech.*, 15, 391-427.
- Makin, V. K., H. Branger, W. L. Peirson and J. P. Giovanangeli (2007) Stress above wind-plus-paddle waves, *J. Phys. Oceanogr.*, 37, 2824-2837.
- Matsunaga, N. and K. Uzaki (2004) The role of wind waves on the formation and development of Langmuir circulation in a shallow water region, *29th International conference on Coastal Engineering*, 1-13.
- McWilliams, J. C., P. P. Sullivan and C. H. Moeng (1997) Langmuir turbulence in the ocean, *J. Fluid Mech.*, 334, 1-30.
- Mitsuyasu, H., (1966) Interactions between water waves and wind (1). *Rep. Res. Ins. Appl. Mech.*, Kyushu Univ., 14, pp. 67-88.
- Mitsuyasu, H. and T. Honda (1982). Wind-induced growth of water waves. *J. Fluid Mech.* 123, 425-442.
- Mitsuyasu, H. (1985) A note on momentum transfer from wind to wave. *Reid Symposium on Practice of Physical Oceanography*, *J. Geophys. Res.* 90, (Paper 4C1339), 3343-3345.

- Mizuno, S. and Z. Cheng (1992). A pair of Langmuir cells in a laboratory tank, *J. oceanogr.* 48, 37-57.
- Mizuno, S., H. Noguchi, and Y. Kimura (1998). A pair of Langmuir cells in two laboratory tanks (II), *J. oceanogr.* 54, 77-100.
- Phillips, O. M. and M. L. Banner (1974) Wave breaking in the presence of wind drift and swell, *J. Fluid Mech.*, 66, 625-640.
- Pollard, R.T. (1977) Observations and theories of Langmuir circulations and their role in near surface mixing. In *A Voyage of Discovery; George Deacon 70th Anniversary Volume*, ed. M. Angel, Oxford, 235-51.
- Polton, J.A., D. M. Lewis, and S. E. Belcher (2005) The role of wave-induced Coriolis-Stokes forcing on the wind-driven mixed layer, *J. Phys. Oceanogr.*, 35, 444-457.
- Polton, J. A. and S. E. Belcher (2007) Langmuir turbulence and deeply penetrating jets in an unstratified mixed layer, *J. Geophys. Res.* 112, C09020, 1-11.
- Smith, J. A. (2006) Observed variability of ocean wave Stokes drift, and the Eulerian response to passing groups, *J. Phys. Oceanogr.*, 36, 1381-1402.
- Thorpe, S. A. (2004) Langmuir circulation, *Annu. Rev. Fluid Mech.*, 36, 55-79.
- Tanno, K. and S. Komori (2004) Effects of swell on turbulence structure and mass transfer across the wind-driven air-water interface [in Japanese], *Transactions of JSME*, B70, 644-649.
- Toba, Y. (1978) Stochastic form of the growth of wind waves in a single-parameter representation with physical implications, *J. Phys. Oceanogr.*, 8, 494-507.